Extracelluar matrix metalloproteinase as a novel target for pancreatic cancer therapy

Hyunki Kim[a,b,g], Guihua Zhai[a], Zhiyong Liu[c], Sharon Samuel[a], Nemil Shah[d], Emily E. Helman[c], Joseph A. Knowles[c], Cecil R. Stockard[e], Naomi S. Fineberg[f], William E. Grizzle[e,g], Tong Zhou[d,g], Kurt R. Zinn[a,d,g] and Eben L. Rosenthal[c,g]

The objective of this study was to evaluate extracellular matrix metalloproteinase (EMMPRIN) as a novel target in orthotopic pancreatic cancer murine models. MIA PaCa-2 human pancreatic tumor cells were implanted in groups 1 and 3–7, whereas MIA PaCa-2 EMMPRIN knockdown cells were implanted in group 2. Dosing with anti-EMMPRIN antibody started immediately after implantation for groups 1–3 (residual tumor model) and at 21 days after cell implantation for groups 4–7 (established tumor model). Groups 3, 5, and 7 were treated with anti-EMMRPIN antibody (0.2–1.0 mg) twice weekly for 2–3 weeks, whereas the other groups served as the control. In the residual tumor model, tumor growth of anti-EMMPRIN-treated group was successfully arrested for 21 days ($15 \pm 4\,mm^3$), which was significantly lower than that of the EMMPRIN knockdown group ($80 \pm 15\,mm^3$; $P=0.001$) or the control group ($240 \pm 41\,mm^3$; $P<0.001$). In the established tumor model, anti-EMMPRIN therapy lowered tumor volume increase by approximately 40% compared with the control, regardless of the dose amount. Ki67-expressed cell density of group 5 was $939 \pm 150\,mm^{-2}$, which was significantly lower than that of group 4 ($1709 \pm 145\,mm^{-2}$; $P=0.006$). Microvessel density of group 5 ($30 \pm 6\,mm^{-2}$) was also significantly lower than that of group 4 ($53 \pm 5\,mm^{-2}$; $P=0.014$), whereas the microvessel size of group 5 ($191 \pm 22\,\mu m^2$) was significantly larger than that of group 4 ($113 \pm 26\,\mu m^2$; $P=0.049$). These data show the high potential of anti-EMMPRIN therapy for pancreatic cancer and support its clinical translation. *Anti-Cancer Drugs* 22:864–874 © **2011 Wolters Kluwer Health | Lippincott Williams & Wilkins.**

Anti-Cancer Drugs 2011, **22**:864–874

Keywords: extracellular matrix metalloproteinase, pancreatic cancer, targeted therapy

Departments of [a]Radiology, [b]Biomedical Engineering, [c]Surgery, [d]Medicine, [e]Pathology, [f]Biostatistics and [g]Comprehensive Cancer Center, University of Alabama at Birmingham, Birmingham, Alabama, USA

Correspondence to Dr Hyunki Kim, G082C Volker Hall, 1670 University Blvd., Birmingham, AL 35294-0012, USA
Tel: +1 205 996 4088; fax: +1 205 975 6522; e-mail: hyunki@uab.edu

Received 10 February 2011 **Revised form accepted** 25 May 2011

Introduction

Pancreatic cancer results in the highest fatality rate of all cancers and is the fourth leading cause of cancer death, regardless of sex and race in the USA. Pancreatic cancer presents with nonspecific and various symptoms, which may lead to late-stage disease at diagnosis, and therefore approximately 85% of newly diagnosed pancreatic cancers are unresectable [1]. Median life expectancy from the time of diagnosis is approximately 3–6 months, and only 4% of patients survive for more than 5 years.

Gemcitabine is the first-line treatment agent for unresectable pancreatic cancer, but its therapeutic efficacy is modest [2]. Although radiation therapy may provide a small benefit of patient survival when combined with gemcitabine [3], dual combination chemotherapy with gemcitabine and any gastrointestinal chemotherapeutic agent such as 5-fluorouracil, cisplatin, irinotecan, or oxaliplatin did not improve survival [4–7]. The triple therapy with 5-fluorouracil, irinotecan, and oxaliplatin presented significant improvement of survival over gemcitabine monotherapy, but the benefit was still minimal [8]. More recently, targeted therapies through anti-epidermal growth factor receptor (EGFR) and anti-vascular endothelial growth factor (VEGF) approaches were investigated. However, cetuximab (anti-EGFR antibody) or bevacizumab (anti-VEGF antibody) in combination with gemcitabine did not present any additive efficacy over gemcitabine monotherapy [9,10], whereas erlotinib (a small molecule targeting EGFR) together with gemcitabine modestly improved the survival [11].

EMMPRIN, also designated CD147 or basigin, is a membrane-bound glycoprotein, highly expressed on most cancer cells, but limited in normal cells [12]. The detailed mechanisms of EMMPRIN are not clearly revealed [13–15], but it is well known that EMMPRIN stimulates the production of matrix metalloproteinases (MMPs) from surrounding stromal cells [16–18]. EMMPRIN promotes MMP production in an autocrine manner as well [19]. MMPs play a pivotal role to degrade extracellular matrix (ECM) components in pancreatic cancer, leading to tumor cell invasion and metastasis [20]. EMMPRIN also elevates urokinase-type plasminogen activator and its receptor of both endothelial and tumor cells, actively involving with ECM degradation

0959-4973 © 2011 Wolters Kluwer Health | Lippincott Williams & Wilkins DOI: 10.1097/CAD.0b013e328349311e

process [21]. Furthermore, EMMPRIN derives tumor neovascularization through stimulating VEGF isoforms and their receptor VEGF receptor-2 by stimulating hypoxia-inducible factor [22]. In one study, EMMPRIN expression was positively correlated with tumor progression and with decreased tumor-specific survival [23]. Of interest, pancreatic cancer expresses high levels of EMMPRIN (87%) [12], and it is surrounded by extremely rich and dense fibrotic stroma [19,24]. Anti-EMMPRIN therapy inhibits the expression and function of monocarboxylate transporters, which prevents the lactate production from cells and thereby reduces the tumor invasion [25]. Efficacy of the anti-EMMPRIN approach using monoclonal antibody (CNTO3899; Centocor Ortho Biotech Inc., Horsham, Pennsylvania, USA) was recently confirmed for head and neck squamous cell carcinoma [26,27]. All of these findings strongly suggest EMMPRIN as a promising target for effective pancreatic cancer treatment.

We developed a novel murine monomeric monoclonal antibody (IgG1 κ; clone name: 1A6) specifically targeting human EMMPRIN, and the subject of this report was to test the feasibility of anti-EMMPRIN therapy for pancreatic cancer using animal models longitudinally with ultrasound imaging (USI), T2-weighted magnetic resonance imaging (T2W MRI), and diffusion-weighted imaging (DWI). Although high anticancer effect of CNTO3899 was demonstrated in in-vitro [26] or ex-vivo setups [27], the therapeutic efficacy should be revalidated with in-vivo animal models. Furthermore, orthotopic implantation is important to reflect the unique environment of primary pancreatic cancer, which may improve the predictability of human tumor response. We used two orthotopic pancreatic cancer xenograft animal models, a postsurgical residual tumor model, and an established solid tumor model.

High-frequency, B-mode, two-dimensional (2D) USI is a time-efficient and cost-efficient noninvasive in-vivo imaging method, enabling longitudinal measurement of abdominal tumor volume [28], and was previously used to measure the sizes of orthotopic pancreatic tumor xenografts after anti-DR5 therapy and chemotherapy [29,30]. T2W MRI is also a noninvasive imaging technique to assess tumor volume [31]. In contrast to 2D USI, T2W MRI can capture the three-dimensional image of the entire tumor mass. The accuracy of tumor volume measurement by T2W MRI was compared with that by USI. DWI is a physiologic MRI technique; the extracellular water is increased during early apoptosis and/or necrosis of cancer cells, raising intratumoral apparent diffusion coefficient (ADC) values, which can be measured by DWI in high sensitivity [32–35]. DWI was successfully applied for orthotopic pancreatic cancer xenografts to evaluate early therapy response [36]. Increased apoptosis was recently observed in head and neck squamous cell carcinoma responding to anti-EMMPRIN therapy [27]. DWI and subsequent histological validation were performed to assess whether apoptosis is induced by anti-EMMPRIN therapy in the established pancreatic cancer murine model.

Materials and methods

Reagents and cell lines

All reagents were from Fisher (Pittsburg, Pennsylvania, USA), unless otherwise specified. Purified monomeric monoclonal anti-EMMPRIN antibody (mouse origin IgG1 K) was provided by Dr Tong Zhou (UAB, Birmingham, Alabama, USA). Fresh Tc-99m pertechnetate was purchased from Birmingham Nuclear Pharmacy (Birmingham, Alabama, USA). The human pancreatic cell line, MIA PaCa-2, was a gift from Dr M. Hollingsworth (University of Nebraska). MIA PaCa-2 cells were cultured in Dulbecco's modified Eagle's medium (DMEM; Mediatech Inc., Herndon, Virginia, USA) supplemented with 10% fetal bovine serum (Hyclone, Logan, Utah, USA).

Extracellular matrix metalloproteinase reduction (knockdown) in MIA PaCa-2 cells

Short hairpin RNA (shRNA) lentiviral particle delivery system was used to generate EMMPRIN knockdown MIA PaCa-2 tumor cell lines according to the manufacturer's instructions (Clontech, Mountain View, California, USA) as follows: DNA oligonucleotide (listed below) specifically targeting EMMPRIN was cloned into pLVX-shRNA1 vector. The vector with EMMPRIN shRNA was subsequently packaged into lentiviral particles. The lentiviral particles were then transduced into MIA PaCa-2 cells, whereas the control MiaPaCa-2 cells were transduced with an empty vector control plasmid. MiaPaCa-2 cells with either vector control or shRNA EMMPRIN were derived from pools of cells resistant to puromycin. After selection under puromycin (1 μg/ml), the drug-resistant cells were assessed using a flow cytometer (Accuri C6; Accuri Cytometers Inc., Ann Arbor, Michigan, USA) for EMMPRIN expression and were further confirmed by western blot. DNA sequences used for targeting EMMPRIN are as follows:

SiE: GCAGCACCAGAATGACAAATTCAAGAGATTTG TCATTCTGGTGCTGCTTTTTTG

Succinimidyl 6-hydrazinonicoinate conjugation and radiolabeling

Succinimidyl 6-hydrazinonicoinate (HYNIC) conjugation and radiolabeling were conducted for in-vitro binding assay by Scatchard analysis. Fresh 1.8 mmol/l solution of HYNIC (courtesy of Dr Gary Bridger, AnorMED Inc., Langley, British Columbia, Canada) in dimethylformamide was prepared. Forty picomoles was transferred to glass vials followed by freezing at −90°C, and then the solutions were vacuum dried using an Advantage Bench-top Freeze Dryer (Virtis Co. Inc., Gardiner, New York, USA)

with the shelf temperature at −75°C and trap at −90°C. The vials were sealed under vacuum and kept frozen at −80°C until use. Each vial was reconstituted with 1.0 ml of sodium phosphate buffer (0.15 mol/l; pH 7.80) containing 1 mg of anti-EMMPRIN antibody (HYNIC/antibody molar ratio = 6). After a 3-h incubation at room temperature, the mixture was transferred to a Slide-A-Lyzer dialysis cassette with a molecular weight cutoff of 10 000 (Pierece, Rockford, Illinois, USA) and then immersed into 1000 ml of phosphate-buffered saline (PBS, pH 7.4) overnight at 4°C. The radiolabeling yield was approximately 60%. The HYNIC-modified anti-EMMPRIN antibody was labeled with Tc-99m using $SnCl_2$/tricine as the transfer ligand [37], and the unbound Tc-99m was removed by G-25 Sephadex size-exclusion chromatography. The protein concentrations of the collected fractions were measured by the assay conducted by Lowry *et al.* [38]. The level of Tc-99m binding to anti-EMMPRIN antibody was greater than 95%, as measured by thin layer chromatography using separate strips eluted with saturated saline and methyl ethyl ketone.

In-vitro binding assay

MIA PaCa-2 cells (or EMMPRIN knockdown MIA PaCa-2 cells) were plated in separate 24-well plates, respectively (500 000 cells per well) and incubated overnight at 37°C in culture medium (DMEM, with 2 mmol/l of L-glutamine, 1 mmol/l of sodium pyruvate, 10% fetal bovine serum; pH 7.4; 0.2 ml/well). The Tc-99m-labeled anti-EMMPRIN antibody was diluted in binding buffer (DMEM, with 30 mmol/l of HEPES, 2 mmol/l of L-glutamine, 1 mmol/l of sodium pyruvate, 1% bovine serum albumin; pH 7.4) to seven to eight concentrations; the highest incubation concentration was approximately 1 nmol/l, with 2-fold subsequent dilutions. Each concentration was in duplicate; a third well at each concentration included excess unlabeled anti-EMMPRIN antibody (41.6 μg per well) for blocking. This control was needed to measure nonspecific binding. The Tc-99m-anti-EMMPRIN antibody was incubated with the live, attached cells for 1 h at 37°C. The free Tc-99m anti-EMMPRIN antibody (not bound to cells) was washed off with 0.2 ml of ice-cold Hank's Balanced Salt Solution (pH 7.2), and 0.2 ml of $NaC_2H_3O_2$–Hank's Balanced Salt Solution (pH 4.0) was added to each well and incubated for 5 min at room temperature to isolate the acid-labile component, presumably the surface-bound component. After the acid-labile fraction was collected, 0.2 ml of NaOH (1 mol/l) was added to each well and incubated for 10 min at room temperature to isolate the binding component that was not removed with the original acid wash. This binding component was referred to as the acid-stable component, and was obtained by dissolving the cells. This component would represent internalized antibody, or surface-bound antibody that was resistant to the acid washing. All acid-stable fractions were assayed for protein concentration, as were known numbers of cells to determine the protein content. The Tc-99m activity in the samples was measured using a γ-ray counter (MINAXIγ Auto-gamma 5000 series Gamma Counter manufactured by Packard Instrument Company, Grove, Illinois, USA). The binding assays were repeated three times independently per cell line. The data were analyzed using Graphpad Prism (version 4.0, San Diego, California, USA) after correction of Tc-99m for decay, and after correction for nonspecific binding. Data were fitted with nonlinear regression analyses assuming one site of binding, enabling the determination of the binding affinity (K_d) and the number of EMMPRIN (assuming 1 antibody per EMMPRIN) [39,40]. As total cells were known, the EMMPRIN number per cell could be determined.

Animal modeling

Animal experiments were reviewed and approved by the Institutional Animal Care and Use Committee. Seven groups of female SCID BALB/c mice (NCI-Frederick Animal Production Program, Fredrick, Maryland, USA; 4–6 weeks old; $n = 12$ for groups 1 and 2, $n = 10$ for group 3, $n = 7$ for group 4, $n = 6$ for group 5, and $n = 5$ for groups 6 and 7) were used. MIA PaCa-2 cells were implanted into groups 1 and 3–7, whereas EMMPRIN knockdown MIA PaCa-2 tumor cells were implanted into group 2. The procedure for intrapancreatic tumor implantation was as follows: a 1-cm incision was made in the left upper quadrant of the abdomen of anesthetized mice, and a solution of 2.5×10^6 MIA PaCa-2 cells (or EMMPRIN knockdown MIA PaCa-2 cells) in 30 μl of DMEM was injected into the tail of the pancreas. The skin and peritoneum were closed in a layer with two interrupted 5–0 Prolene sutures. For groups 1–3, dosing and imaging were started immediately after cell implantation to model postsurgical residual tumors, whereas, for groups 4–7, these were started at 21 days after cell implantation to model established pancreatic tumors. Groups 1 and 2 were intraperitoneally injected with PBS, whereas group 3 was intraperitoneally injected with anti-EMMPRIN antibody (0.2 mg), twice weekly for 3 weeks with weekly USI. Groups 4 and 5 were intraperitoneally injected with PBS (serving as control) and anti-EMMPRIN antibody (0.2 mg), respectively twice weekly for 3 weeks with weekly USI. Groups 6 and 7 were intraperitoneally injected with PBS and anti-EMMPRIN antibody (1 mg), respectively twice weekly for 2 weeks, with weekly USI, T2W MRI, and DWI; USI was applied for all animals of groups 3 and 4, whereas T2W MRI and DWI were applied for randomly selected animals ($n = 3$ from group 6, $n = 4$ from group 7). All animals were anesthetized using isoflurane gas (1–2%) during imaging.

Ultrasound imaging

USI was performed using a VisualSonics VEVO 660 high-frequency, high-resolution ultrasound instrument with a 40-MHz probe (Toronto, Ontario, Canada). Animals were placed in the supine position for examination with B-mode imaging [28]. The largest diameter was found

in the anterior–posterior plane, and this diameter as well as a transverse diameter were measured. Then, the ultrasound probe was rotated 90° to measure the largest diameter in the sagittal plane. The tumor volume was calculated using the following equation, volume $= xyz(\pi/6)$, where x, y, and z are the three orthogonal diameters of a tumor. US-image acquisition and analysis were conducted in a blinded manner.

Magnetic resonance imaging

Small animal T2W MRI and DWI were performed on a Bruker BioSpec 9.4T system (Bruker BioSpin Corp., Billerica, Massachusetts, USA). The animal was placed in an animal bed equipped with circulating warm water to regulate body temperature during scans. An orthogonally bent plastic board was used to prevent the transfer of the respiratory motion in the chest-to-abdominal area. Tumor was imaged using a combination of a 1H volume resonator/transmitter and a surface coil receiver (Bruker BioSpin Corp.). An magnetic resonance-compatible small animal respiratory gating device (SA Instrument Inc., Stony Brook, New York, USA) was used during scans. T2W MRI was performed using a spin-echo sequence (Rapid Acquisition with Relaxation Enhancement) with the following acquisition parameters: repetition time/echo time = 2000/48.8 ms, 128×128 matrix, and a 30×30-mm field of view. Continuous 1 mm-thick slices were used to cover the entire tumor region. DWI data were collected using a standard spin-echo sequence with four b-factors (5, 300, 600, and 1000 s/mm^2). The acquisition parameters are as follows: repetition time/echo time = 2500/32 ms, diffusion separation time = 16 ms, diffusion gradient duration = 6 ms, 128×128 matrix, and a 30×30-mm field of view. A total of three to five 1 mm-thick slices were acquired to cover tumor regions of interest in an interlaced mode. Tumor volume was measured by summing all voxels inside the tumor boundary of T2W MR images. Segmentation of the tumor volume was performed based on the signal intensity between the region of interest and the background using ImageJ, version 1.40g (National Institutes of Heath, Bethesda, Maryland, USA). The ADC value of each pixel of the segmented tumor region was determined from the best-fitting linear function, $\ln I_b = \ln I_0 - (\mathrm{ADC} \times b)$, where I_b was the intensity on the pixel with b, and I_0 was the intensity on the pixel with $b = 0$. The final ADC value of a tumor was obtained by averaging all ADC values in the entire tumor region. The ADC and tumor volume quantification were implemented using computer software developed with Labview, version 8.5 (National Instruments Co., Austin, Texas, USA).

Histological analyses

At day 42, terminal deoxynucleotidyl transferase dUTP nick-end labeling (TUNEL), Ki67, and CD31 staining were performed for tumor tissues of groups 4 and 5 ($n = 5$ selected randomly per group), with the same procedure as reported previously [41,42]. Two digital microphotographs were taken away from areas of necrosis, but were otherwise randomly selected for each tumor slice that had undergone TUNEL ($\times 100$), Ki67 ($\times 100$), or CD31 ($\times 200$) staining, using SPOT camera on an Olympus 1×70 microscope (Olympus Optical Co., Tokyo, Japan), interfaced with a personal computer and SPOT software. The apoptotic (TUNEL) or proliferating (Ki67 expressing) cells were segmented by the signal-intensity difference between the target cells and background in each photograph, whereas the intensity and minimum particle size thresholds were determined manually. Then, the target cells were counted, and the cell density (cell number/mm^2) was calculated. The cell densities of the two photographs for each tumor slide were averaged. The CD31-stained area was segmented in the same way, and the area fraction (CD31-stained area/total area), considered as endothelial cell density, was calculated. Furthermore, the number and size of microvessels were quantified, and the microvessel density (vessel number/mm^2) and microvessel size (μm^2) are presented. The image analysis was performed using ImageJ, version 1.40g (National Institute of Heath).

Statistical analyses

One-way analyses of variance (ANOVAs) was carried out using SAS, version 9.2 (SAS Institute Inc., Cary, North Carolina, USA) to compare MIA PaCa-2 versus EMMPRIN knockdown MIA PaCa-2 cells for binding affinity of Tc-99m-anti-EMMPRIN antibody (K_d) and EMMPRIN number per cell [43]. ANOVA was also used for comparison of proliferating or apoptotic cell densities. SPSS, version 16.0 (SPSS Inc., Chicago, Illinois, USA) was used to compare tumor volume (or ADC) changes among groups over 2–3 weeks using two-way repeated measures of ANOVA [44]. P values of less than 0.05 were considered significant. Data are presented as mean ± standard error.

Results

Flow cytometry and western blotting analyses

To evaluate the function of EMMPRIN in pancreatic tumor growth and progression, MIAPaCa-2 stably silenced for EMMPRIN expression (SiE), as well as cells with vector as control, were generated. The EMMPRIN expression of these cells was verified by flow cytometry and by western blot (Fig. 1a and b). EMMPRIN level of SiE-silenced cells are 29.3% of that of vector as control cells, which is generated by comparison of immunofluorescence and western blot band densities.

In-vitro binding assay

An in-vitro binding assay determined the specific binding affinity (K_d) of Tc-99m-labeled anti-EMMPRIN antibody and the number of EMMPRIN per cell for MIA PaCa-2 or EMMPRIN knockdown MIA PaCa-2 cells. Figure 2 shows representative Scatchard plots for Tc-99m–anti-EMMPRIN

Fig. 1

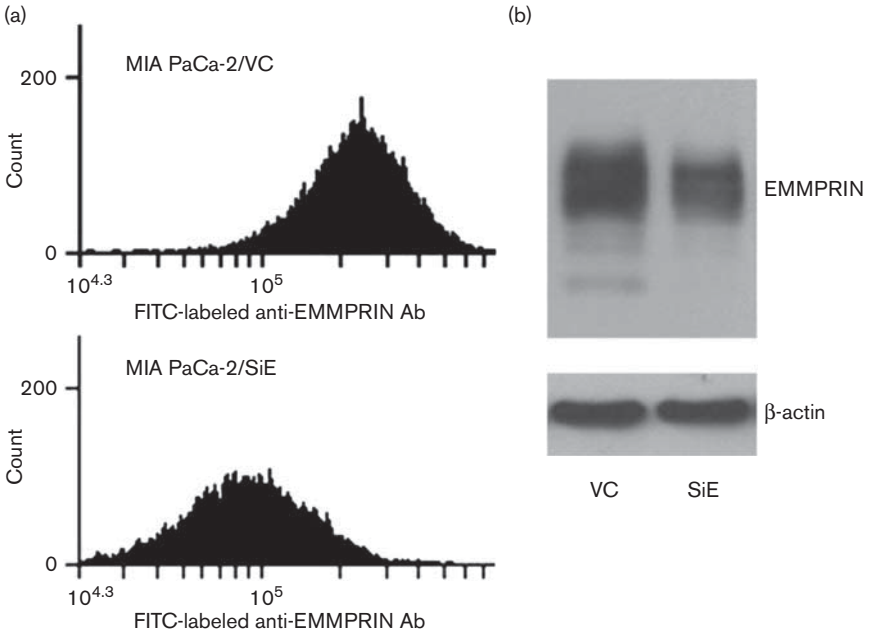

Validation of EMMPRIN expression. (a) Extracellular matrix metalloproteinase (EMMPRIN) expression evaluated by flow cytometry, when MIAPaCa-2 was transduced by lentiviral particles carrying vectors with EMMPRIN short hairpin RNA SiE1 or vector as control (VC). The cells were stained with fluorescein isothiocyanate (FITC)-conjugated anti-human EMMPRIN antibodies. (b) Verification of EMMPRIN expression by western blotting assay. Cell lysates from control cells as well as from EMMPRIN-silenced cells were subjected to western blotting using antibody against EMMPRIN. β-actin was used as a loading control.

antibody binding to EMMPRIN expressed on (a) MIA PaCa-2 and (b) EMMPRIN knockdown MIA PaCa-2 cells, after correction for nonspecific binding (insets are saturation binding curves). The K_d for the acid-stable binding component in MIA PaCa-2 cell line was 4.31 ± 0.59 nmol/l, which was not significantly different from that in the EMMPRIN knockdown MIA PaCa-2 cell line (2.83 ± 0.27 nmol/l; $P = 0.084$). However, the number of EMMPRIN per cell was $582\,000 \pm 56\,000$ for MIA PaCa-2 cells, which was significantly higher than for EMMPRIN knockdown MIA PaCa-2 cells ($220\,000 \pm 89\,000$; $P = 0.026$). The acid-labile binding components were too small to be quantitatively assessed in both the cell lines (data not shown).

In-vivo ultrasound imaging

In-vivo USI detected high therapeutic efficacy of anti-EMMPRIN antibody for both the postsurgical residual and for established MIA PaCa-2 tumor models. Figure 3a shows the representative ultrasound image of an orthotopic pancreatic tumor xenograft, showing two orthogonal dimensions and tumor boundary with a white dotted circle. Figure 3b shows the tumor volume changes of groups 1–3 (postsurgical residual tumor model) for 3 weeks after therapy initiation. The tumor volumes of groups 1–3 on day 15 were 66 ± 17, 21 ± 5, and $4 \pm 2\,mm^3$ respectively, and 240 ± 41, 80 ± 15, and $15 \pm 4\,mm^3$, respectively on day 21; tumor growth of group 3 treated with anti-EMMPRIN antibody was significantly lower than that of the control group (group 1; $P < 0.001$) or the EMMPRIN knockdown group (group 2; $P = 0.001$), whereas tumor growth of group 2 was also significantly lower than that of group 1 ($P = 0.002$).

Figure 3c shows the tumor volume changes of groups 4 and 5 (established tumor model) for 3 weeks after therapy initiation, when the tumor volumes were normalized to the values on day 21; the mean tumor volume of the two groups on day 21 was $85 \pm 9\,mm^3$ without statistical difference ($P = 0.500$). The tumor volume changes of group 4 were 182 ± 33, 395 ± 107, and $625 \pm 166\%$ on days 28, 35, and 42 respectively, whereas those of group 5 were 91 ± 7, 163 ± 27, and $329 \pm 39\%$ respectively during the same time. The tumor volume increase was approximately 40% reduced by anti-EMMPRIN therapy in average, but not statistically significant ($P = 0.083$).

Figure 3d shows the tumor-volume changes of groups 6 and 7 for 2 weeks after therapy initiation, testing the higher dose of anti-EMMPRIN antibody (1 mg) in the established tumor model; the tumor volumes were normalized to the values on day 21, and the mean tumor volume of the two groups was $142 \pm 11\,mm^3$ on day 21 without statistical difference ($P = 0.230$). The tumor volume changes of group 6 were 217 ± 55 and $405 \pm 96\%$

Fig. 2

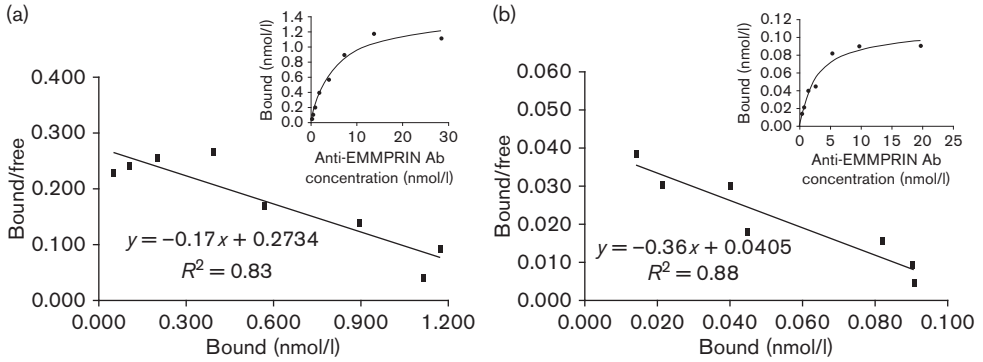

Representative scatchard plots of Tc-99m-labeled anti-extracellular matrix metalloproteinase (EMMPRIN) antibody binding to (a) MIA PaCa-2 cells or (b) EMMPRIN knockdown MIA PaCa-2 cells (the acid-stable binding components are shown). Inserts are saturation binding curves.

on days 28 and 35, respectively, whereas those of group 7 were 89 ± 27 and $144 \pm 41\%$, respectively during the same time. The tumor volume increase of group 7 was approximately 46% lower than that of group 6 with statistical significance ($P = 0.043$).

In-vivo magnetic resonance imaging

In-vivo T2W MRI presented that the tumor volume change after anti-EMMPRIN treatment was significantly lower than that of the control group in higher accuracy than USI did, although intratumoral ADC increase was not detected. Figure 4a shows a representative set of DW images at four *b* values (5, 300, 600, and 1000 s/mm^2) with the same gray scaling, and the ADC map calculated from the DW images; tumor location is indicated with a white arrow in the first subfigure. Figure 4b shows the tumor volume changes of mice randomly selected from groups 6 ($n = 3$) and 7 ($n = 4$) for 2 weeks postdose initiation, analyzed using T2W MR images. The tumor volume changes of group 6 were 153 ± 30 and $334 \pm 52\%$ on days 28 and 35, respectively, whereas those of group 7 were 46 ± 11 and $112 \pm 11\%$, respectively during the same time, with statistical difference between the two groups ($P = 0.002$); the averaged coefficient of variation of tumor volume changes on each time point relative to day 21 was 0.32 ± 0.06 ($n = 4$; $n = 2$ per each time point), which was significantly lower than that analyzed by USI shown in Fig. 3d (0.61 ± 0.04; $P = 0.005$), showing an improved accuracy of tumor volume assessment. Figure 4c shows the intratumoral ADC changes of groups 6 and 7 for 2 weeks after treatment initiation; the mean ADC value of the two groups on day 21 was 0.00100 ± 0.00008 mm^2/s without statistical difference ($P = 0.437$). The averaged ADC values of both the groups decreased over time, whereas the magnitude of ADC decrease of group 6 was approximately 10% lower than that of group 7 on either day, but was not statistically different ($P = 383$).

Histological analysis

Histological analysis detected the significantly reduced tumor cell proliferation and microvessel density due to anti-EMMPRIN therapy, but did not detect the change of apoptotic cell density. Figure 5a shows the representative microphotographs of Ki67-stained, TUNEL-stained, and CD31-stained tumor slices (5-μm thickness) of groups 4 and 5, whereas the proliferating (Ki67 stained), apoptotic (TUNEL stained), and endothelial (CD31 stained) cells are indicated with black arrows in each subfigure. Figure 5b shows the Ki67-expressed cell densities (cell number/mm^2) of groups 4 and 5 ($n = 5$ per group), and that of group 4 was 1709 ± 145 mm^{-2}, which was significantly higher than that of group 5 (939 ± 150 mm^{-2}; $P = 0.006$). Figure 5c shows the TUNEL-stained cell densities (cell number/mm^2) of groups 4 and 5, and that of group 4 (81 ± 14 mm^{-2}) was not statistically different from that of group 5 (81 ± 15 mm^{-2}; $P = 0.994$). Figure 5d shows the microvessel densities (vessel number/mm^2) and microvessel size (μm^2) of groups 4 and 5; microvessel density of group 5 (60 ± 11 mm^{-2}) was significantly lower than that of group 4 (106 ± 10 mm^{-2}; $P = 0.014$), whereas the microvessel size of group 5 (323 ± 37 μm^2) was significantly larger than that of group 4 (190 ± 43 μm^2; $P = 0.049$). The endothelial cell density of group 5 ($1.07 \pm 0.12\%$) was also significantly lower than that of group 4 ($1.62 \pm 0.16\%$; $P = 0.0376$).

Discussion

To our knowledge, this is the first report of anti-EMMPRIN therapy in pancreatic cancer murine models. Of note, higher antitumor effect was demonstrated in the postsurgical residual tumor model. Anti-EMMPRIN therapy prevents remodeling of ECM for neovascularization [22], and therefore avascular tumor growth can be

Fig. 3

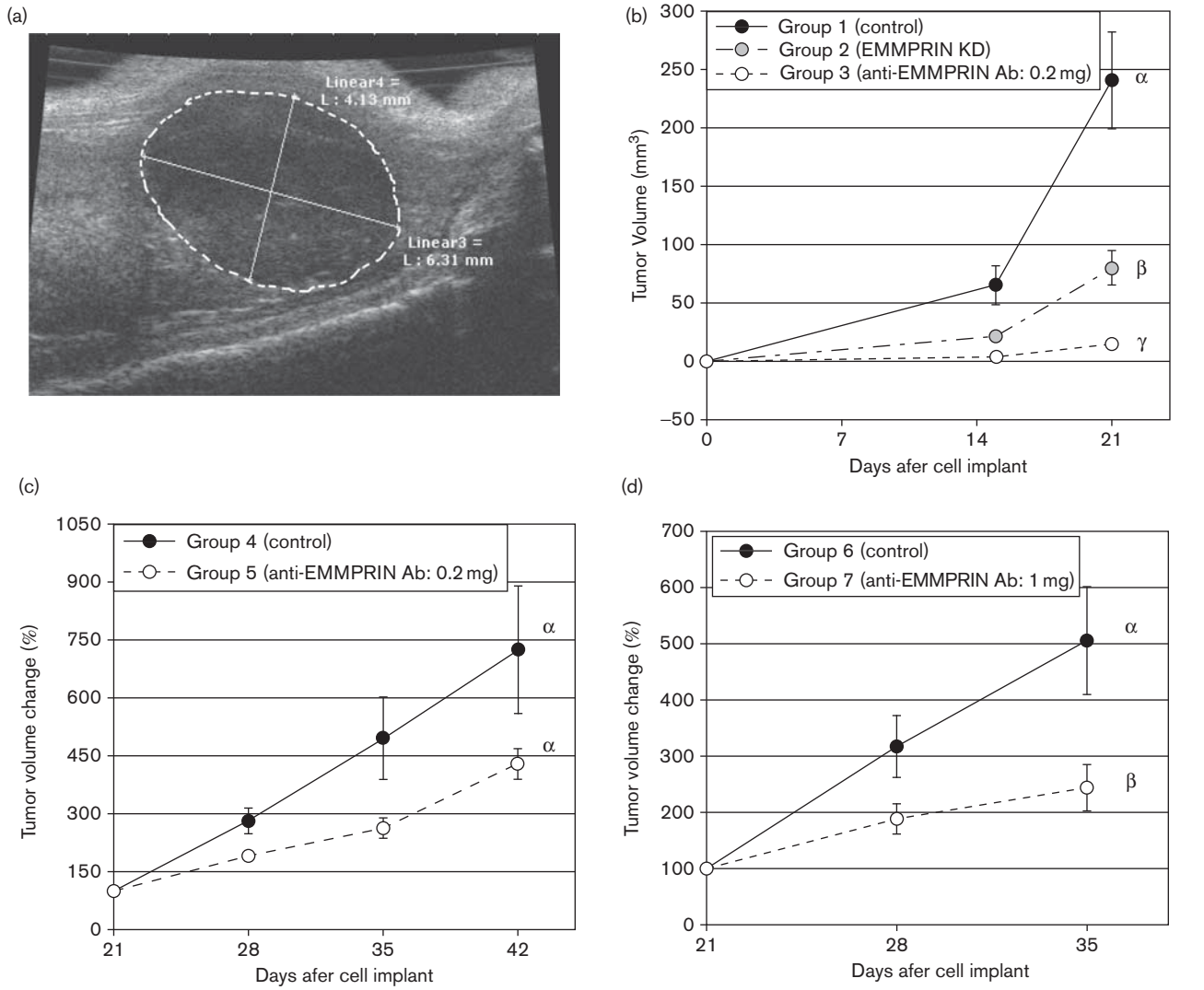

In-vivo ultrasound image analysis of tumor response. (a) Representative two-dimensional ultrasound image of an orthotopic pancreatic tumor xenograft showing two orthogonal dimensions, whereas the tumor boundary is indicated with a white dotted circle. (b) Tumor volume change after intraperitoneal injection of phosphate-buffered saline (PBS) (groups 1 and 2) or 0.2 mg of anti-extracellular matrix metalloproteinase (EMMPRIN) antibody (group 3) twice weekly for 3 weeks when dosing started immediately after cell implantation (postsurgical residual tumor model). (c) Tumor volume changes after intraperitoneal injection of PBS (group 4) or 0.2 mg of anti-EMMPRIN antibody (group 5) twice weekly for 3 weeks, when dosing started at 21 days after cell implantation (established tumor model). (d) Tumor volume changes after intraperitoneal injection of PBS (group 6) or 1 mg of anti-EMMPRIN antibody (group 7) twice weekly for 2 weeks, when dosing started at 21 days after cell implantation. Different Greek letters represent statistical difference among the groups during the entire therapy period.

effectively constrained. However, once a tumor enters the vascular phase and the surrounding ECM is degraded, the growth control by the anti-EMMPRIN approach might be diminished. Thus, anti-EMMPRIN therapy will be presumably most effective in adjuvant setting or for tumor prevention. The EMMPRIN knockdown tumor cells had a 62% reduction in the number of EMMRPIN per cell on average by the in-vitro assay, which is comparable with in-vivo data showing a 67% smaller size on average of EMMPRIN knockdown tumors than those of control tumors on either day 15 or 21. These data support the proposed mechanism that the antitumor growth effect was mainly dependent on blocking the extracellular signaling of EMMPRIN. A biodistribution study of anti-EMMPRIN antibody was performed, and no significantly higher uptakes were noticed in any normal organs except spleen (data not shown). This may represent the possibility that anti-EMMPRIN antibody has cross-reactivity on murine monocyte and potential toxicity against it, but more studies will need to be followed to validate it.

Anti-EMMPRIN therapy lowered pancreatic cancer cell proliferation and microvessel density; 43% of microvessel

Fig. 4

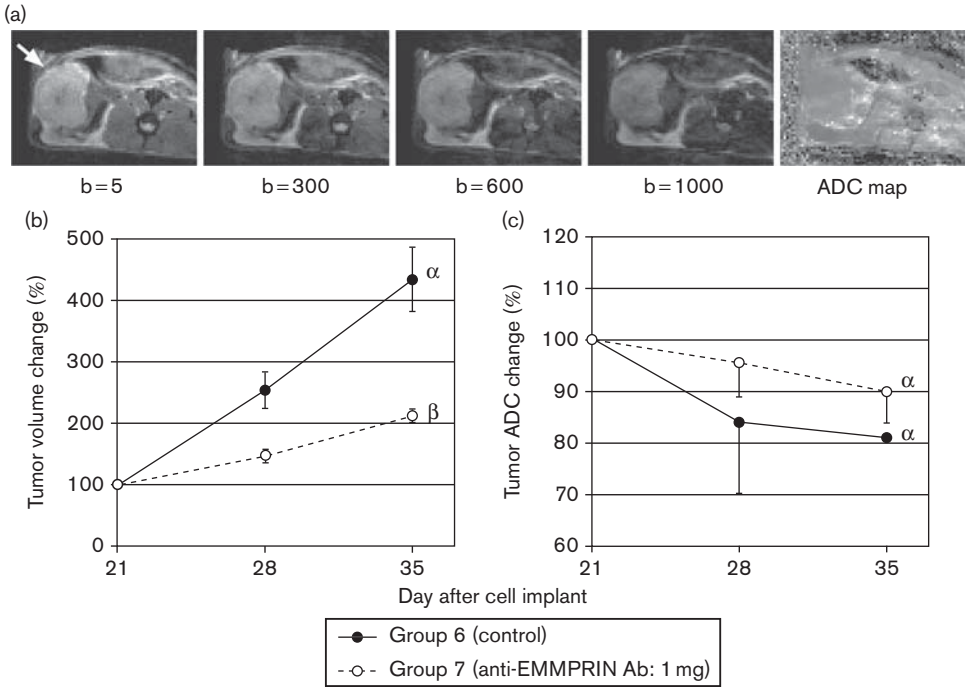

(a) Representative diffusion-weighted images in the same intensity scale at four different *b* values (5, 300, 600, 1000 s/mm^2) and apparent diffusion coefficient (ADC) map of an orthotopically implanted MIA PaCa-2 tumor xenograft; tumor location is indicated with a white arrow. (b) Tumor volume or (c) intratumoral ADC changes (%) of mice randomly selected from groups 6 ($n=3$) and 7 ($n=4$), which were intraperitoneally injected with phosphate-buffered saline and anti-extracellular matrix metalloproteinase (EMMPRIN) antibody (1.0 mg) twice weekly for 2 weeks, respectively. Different Greek letters represent statistical difference between groups 6 and 7 during 2 weeks.

density was reduced, which is fairly comparable with the 45% decrease of cell proliferation. This may indicate that the antiangiogenic effect induced by anti-EMMPRIN antibody could be a major cause for the growth suppression of the established tumors. Of interest, the mean microvessel size was significantly larger when treated with anti-EMMPRIN antibody. This is primarily due to the suppression of neovascularization; the averaged vessel size would be larger when small vessels were not present. Furthermore, antineovascularization may release the tumor interstitial pressure, and thereby expand the compressed vessels.

However, anti-EMMRPIN therapy did not induce apoptosis as shown in ADC and histological analyses. We also implemented an in-vitro cell-viability assay using two different human pancreatic cancer cell lines, MIA PaCa-2 and PANC1, but no cytotoxic efficacy of anti-EMMPRIN therapy was measured (data not shown). However, activated caspase-3 and DNA fragmentation were increased when EMMPRIN was knocked down in breast cancer cells [45], and more recently an increased apoptosis after anti-EMMPRIN therapy was observed in 17 human head and neck tumor tissues among a total of 22 samples (77%) [27]. Bougatef *et al.* [46] demonstrated that EMMPRIN inhibited melanoma cell apoptosis, while promoting migration and proliferation of these cells by upregulating VEGF receptor-2. Perhaps EMMPRIN may minimally function for apoptosis control in pancreatic cancer cells, while future studies with various pancreatic cancer cell lines should be followed for better understanding of this data inconsistency. The decrease of intratumoral mean ADC values over time is presumably due to the increase of cell density in pancreatic tumor xenografts, which was observed in our previous study as well [36].

We used only one human pancreatic cancer cell line, MIA PaCa-2, in the in-vivo animal studies for comparison with our previous anti-DR5 and anti-EGFR studies using the same cell line [36,47]. However, as the therapeutic effect of anti-EMMPRIN antibody is modest in the established solid tumor model, the antibody effect for nonresectable pancreatic tumors may need to be further validated using more human pancreatic cancer cell lines. Ideally, it will be necessary to use a pancreatic tumorgraft model to predict human cancer response with greater accuracy; the tumors that directly transferred from patients into animals without the culturing process, called tumorgraft, closely mirror the primary tumors. The tumorgrafts created by Fiebig *et al.* [48] predicted a sensitive response in 90% and a resistant response in 97% of patients, and we are currently developing the pancreatic tumorgraft modes for evaluating anti-EMMPRIN antibody.

Fig. 5

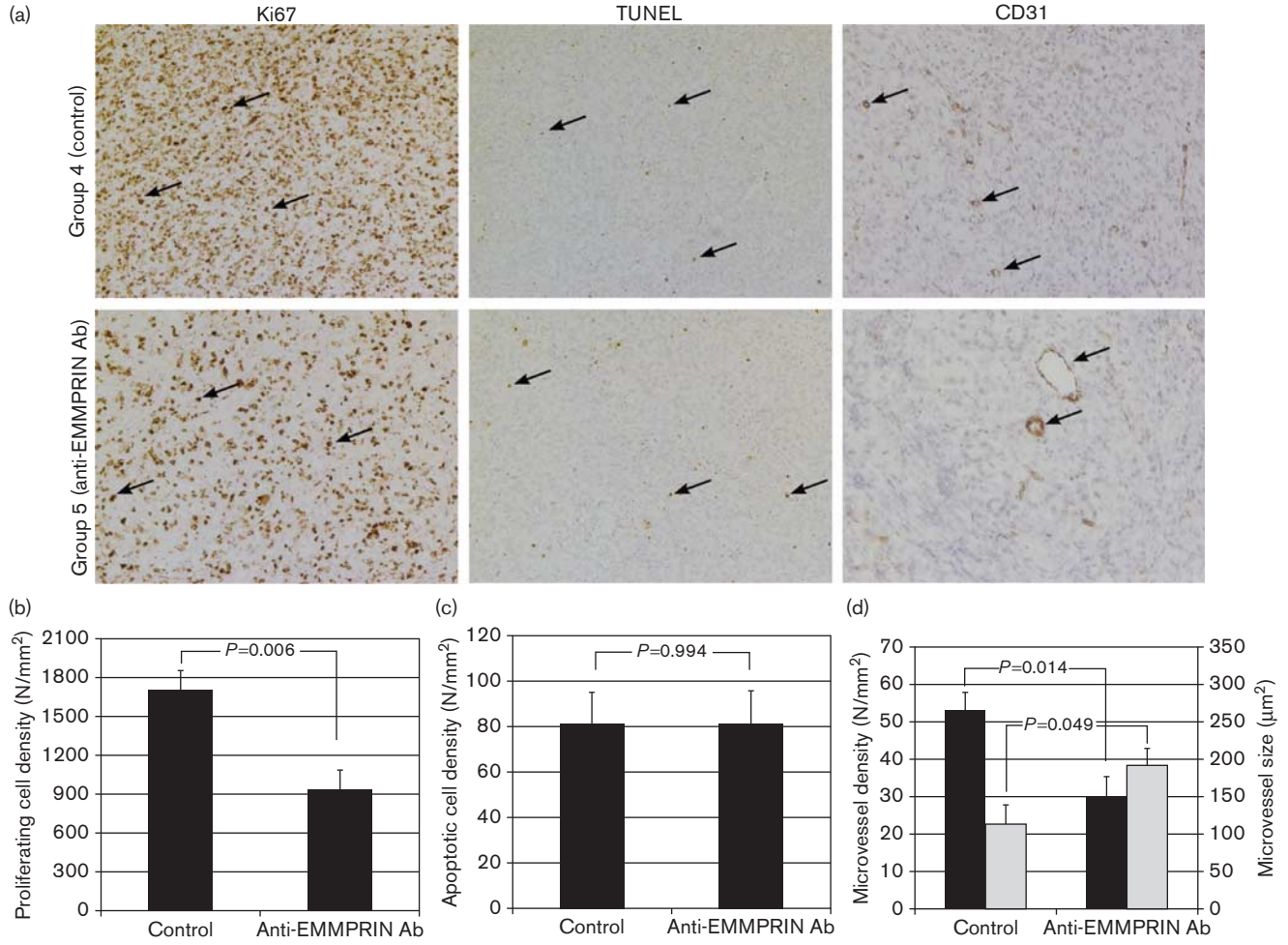

Histological analysis of tumor response. (a) Representative Ki67-stained (× 100), terminal deoxynucleotidyl transferase dUTP nick-end labeling (TUNEL)-stained (× 100), and CD31-stained (× 200) slices of MIA PaCa-2 tumors collected on day 42, when the intraperitoneal injection of phosphate-buffered saline (PBS, group 4) or 0.2 mg of anti-extracellular matrix metalloproteinase (EMMPRIN) antibody (group 5) started on day 21 twice weekly for 3 weeks. Proliferating (Ki67 stained), apoptotic (TUNEL stained), and endothelial (CD31 stained) cells are indicated with black arrows in each subslice. (b) Proliferating cell density (cell number/mm^2), (c) apoptotic cell density, and (d) microvessel density and size of groups 4 and 5 with *P* values. In panel d, black bars represent microvessel density, and gray bars represent microvessel size.

The limited expression of EMMPRIN in normal cell types may allow anti-EMMPRIN therapy in combination with other chemotherapeutic agents such as gemcitabine in an acceptable level of side effect [12]. Furthermore, the suppressed angiogenesis through anti-EMMPRIN antibody may improve the normalization of tumor microvasculature, leading to the decrease of tumor interstitial fluid pressure [14], which may enhance the delivery efficiency of a drug when used in combination [49]. An improved drug delivery may result in therapeutic synergy [50]. Anti-EMMPRIN therapy may lead to synergy in combination with DR5-targeted therapy by inducing apoptosis while preventing tumor invasion and metastasis, because anti-DR5 therapy induces DR5 aggregation-triggering apoptosis [51], and because high levels of DR5 expression were observed in pancreatic cancer stem cells [52].

USI assessed the volume of orthotopic pancreatic tumor xenografts longitudinally with good accuracy. The tumor volume changes measured by USI were not significantly different from those by T2W MRI, but the coefficient of variation was approximately twice higher. The statistical significance between groups 4 and 5 could be detected if T2W MRI were used to assess tumor volume, as histological analysis validated the significantly reduced cell proliferation after anti-EMMPRIN therapy. As 2D USI produces a cross-sectional image of an object at an arbitrary angle, higher variability of the size measurement is inevitable. Instead, the hand-free 2D array scanning technique

using a 2D USI probe would be used for capturing the whole tumor volume image with extended acquisition and analysis time, or a 3-dimensional US imager could also be used to improve the measurement accuracy [53].

Acknowledgements

The authors thank Lin Belt, Lee Whitworth, and Amber Martin for assistance with growing cells, in-vitro assays, animal monitoring, and imaging. All experiments complied with current regulatory requirements (including ethics requirements) and with the laws of the United States of America.

Grant support: AACR-PANCAN Career Development Award; HSF-GEF Scholar Award; National Cancer Institute (R01CA142637 and 5K08CA102154); and UAB small animal imaging shared facility (5P30CA013148).

Conflicts of interest

There are no conflicts of interest.

References

1 Wray CJ, Ahmad SA, Matthews JB, Lowy AM. Surgery for pancreatic cancer: recent controversies and current practice. *Gastroenterology* 2005; **128**:1626–1641.
2 Burris HA III, Moore MJ, Andersen J, Green MR, Rothenberg ML, Modiano MR, *et al*. Improvements in survival and clinical benefit with gemcitabine as first-line therapy for patients with advanced pancreas cancer: a randomized trial. *J Clin Oncol* 1997; **15**:2403–2413.
3 Loehrer PJ, Powell ME, Cardenes HR, Wagner L, Brell JM, Ramanathan RK, *et al*. A randomized phase III study of gemcitabine in combination with radiation therapy versus gemcitabine alone in patients with localized, unresectable pancreatic cancer: E4201. *J Clin Oncol* 2008; **26**: (Suppl):4506.
4 Berlin JD, Catalano P, Thomas JP, Kugler JW, Haller DG, Benson AB III. Phase III study of gemcitabine in combination with fluorouracil versus gemcitabine alone in patients with advanced pancreatic carcinoma: Eastern Cooperative Oncology Group Trial E2297. *J Clin Oncol* 2002; **20**:3270–3275.
5 Heinemann V, Quietzsch D, Gieseler F, Gonnermann M, Schönekäs H, Rost A, *et al*. Randomized phase III trial of gemcitabine plus cisplatin compared with gemcitabine alone in advanced pancreatic cancer. *J Clin Oncol* 2006; **24**:3946–3952.
6 Rocha Lima CM, Green MR, Rotche R, Miller WH Jr, Jeffrey GM, Cisar LA, *et al*. Irinotecan plus gemcitabine results in no survival advantage compared with gemcitabine monotherapy in patients with locally advanced or metastatic pancreatic cancer despite increased tumor response rate. *J Clin Oncol* 2004; **22**:3776–3783.
7 Louvet C, Labianca R, Hammel P, Lledo G, Zampino MG, André T, *et al*. Gemcitabine in combination with oxaliplatin compared with gemcitabine alone in locally advanced or metastatic pancreatic cancer: results of a GERCOR and GISCAD phase III trial. *J Clin Oncol* 2005; **23**:3509–3516.
8 Conroy T, Desseigne F, Ychou M, Ducreux M, Bouche O, Guimbaud R, *et al*. Randomized phase III trial comparing FOLFIRINOX [F: 5FU/leucovorin (LV), irinotecan (I), and oxaliplatin (O)] versus gemcitabine (G) as first-line treatment for metastatic pancreatic adenocarcinoma (MPA): preplanned interim analysis results of the PRODIGE 4/ACCORD 11 trial. *J Clin Oncol* 2010; **28**:15s.
9 Xiong HQ, Rosenberg A, LoBuglio A, Schmidt W, Wolff RA, Deutsch J, *et al*. Cetuximab, a monoclonal antibody targeting the epidermal growth factor receptor, in combination with gemcitabine for advanced pancreatic cancer: a multicenter phase II Trial. *J Clin Oncol* 2004; **22**:2610–2616.
10 Kindler HL, Friberg G, Singh DA, Locker G, Nattam S, Kozloff M, *et al*. Phase II trial of bevacizumab plus gemcitabine in patients with advanced pancreatic cancer. *J Clin Oncol* 2005; **23**:8033–8040.
11 Moore MJ, Goldstein D, Hamm J, Figer A, Hecht JR, Gallinger S, *et al*. Erlotinib plus gemcitabine compared with gemcitabine alone in patients with advanced pancreatic cancer: a phase III trial of the National Cancer Institute of Canada Clinical Trials Group. *J Clin Oncol* 2007; **25**:1960–1966.
12 Riethdorf S, Reimers N, Assmann V, McCabe F, Millar H, Rafferty P, *et al*. High incidence of EMMPRIN expression in human tumors. *Int J Cancer* 2006; **119**:1800–1810.
13 Rosenthal EL, Vidrine DM, Zhang W, Kornfeld JW, Terracciano L, Sauter G, *et al*. Extracellular matrix metalloprotease inducer stimulates fibroblast-mediated tumor growth *in vivo*. *Laryngoscope* 2006; **116**:1086–1092.
14 Tang Y, Nakada MT, Kesavan P, McCabe F, Millar H, Rafferty P, *et al*. Extracellular matrix metalloproteinase inducer stimulates tumor angiogenesis by elevating vascular endothelial cell growth factor and matrix metalloproteinases. *Cancer Res* 2005; **65**:3193–3199.
15 Zhang W, Matrisian LM, Holmbeck K, Vick CC, Rosenthal EL. Fibroblast-derived MT1-MMP promotes tumor progression *in vitro* and *in vivo*. *BMC Cancer* 2006; **6**:52.
16 Caudroy S, Polette M, Nawrocki-Raby B, Cao J, Toole BP, Zucker S, *et al*. EMMPRIN-mediated MMP regulation in tumor and endothelial cells. *Clin Exp Metastasis* 2002; **19**:697–702.
17 Braundmeier AG, Fazleabas AT, Lessey BA, Guo H, Toole BP, Nowak RA. Extracellular matrix metalloproteinase inducer regulates metalloproteinases in human uterine endometrium. *J Clin Endocrinol Metab* 2006; **91**:2358–2365.
18 Dalberg K, Eriksson E, Enberg U, Kjellman M, Backdahl M, Gelatinase A. Membrane type 1 matrix metalloproteinase, and extracellular matrix metalloproteinase inducer mRNA expression: correlation with invasive growth of breast cancer. *World J Surg* 2000; **24**:334–340.
19 Zucker S, Hymowitz M, Rollo EE, Mann R, Conner CE, Cao J, *et al*. Tumorigenic potential of extracellular matrix metalloproteinase inducer. *Am J Pathol* 2001; **158**:1921–1928.
20 Ellenrieder V, Alber B, Lacher U, Hendler SF, Menke A, Boeck W, *et al*. Role of MT-MMPs and MMP-2 in pancreatic cancer progression. *Int J Cancer* 2000; **85**:14–20.
21 Quemener C, Gabison EE, Naimi B, Lescaille G, Bougatef F, Podgorniak MP, *et al*. Extracellular matrix metalloproteinase inducer up-regulates the urokinase-type plasminogen activator system promoting tumor cell invasion. *Cancer Res* 2007; **67**:9–15.
22 Bougatef F, Quemener C, Kellouche S, Naimi B, Podgorniak MP, Millot G, *et al*. EMMPRIN promotes angiogenesis through hypoxia-inducible factor-2alpha-mediated regulation of soluble VEGF isoforms and their receptor VEGFR-2. *Blood* 2009; **114**:5547–5556.
23 Reimers N, Zafrakas K, Assmann V, Egen C, Riethdorf L, Riethdorf S, *et al*. Expression of extracellular matrix metalloproteases inducer on micrometastatic and primary mammary carcinoma cells. *Clin Cancer Res* 2004; **10**:3422–3428.
24 Seymour AB, Hruban RH, Redston M, Caldas C, Powell SM, Kinzler KW, *et al*. Allelotype of pancreatic adenocarcinoma. *Cancer Res* 1994; **54**:2761–2764.
25 Schneiderhan W, Scheler M, Holzmann KH, Marx M, Gschwend JE, Bucholz M, *et al*. CD147 silencing inhibits lactate transport and reduces malignant potential of pancreatic cancer cells in *in vivo* and *in vitro* models. *Gut* 2009; **58**:1391–1398.
26 Dean NR, Newman JR, Helman EE, Zhang W, Safavy S, Weeks DM, *et al*. Anti-EMMPRIN monoclonal antibody as a novel agent for therapy of head and neck cancer. *Clin Cancer Res* 2009; **15**:4058–4065.
27 Dean NR, Knowles JA, Helman EE, Aldridge JC, Carroll WR, Magnuson JS, *et al*. Anti-EMMPRIN antibody treatment of head and neck squamous cell carcinoma in an ex-vivo model. *Anti-cancer Drugs* 2010; **21**:861–867.
28 Pezold JC, Zinn K, Talbert MA, Desmond R, Rosenthal EL. Validation of ultrasonography to evaluate murine orthotopic oral cavity tumors. *ORL J Otorhinolaryngol Relat Spec* 2006; **68**:159–163.
29 Derosier LC, Buchsbaum DJ, Oliver PG, Huang Z, Sellers JC, Grizzle WE, *et al*. Combination treatment with TRA-8 anti death receptor 5 antibody and CPT-11 induces tumor regression in an orthotopic model of pancreatic cancer. *Clin Cancer Res* 2007; **13**:5535s–5543s.
30 Derosier LC, Vickers SM, Zinn KR, Huang Z, Wang W, Grizzle WE, *et al*. TRA-8 anti-DR5 monoclonal antibody and gemcitabine induce apoptosis and inhibit radiologically validated orthotopic pancreatic tumor growth. *Mol Cancer Ther* 2007; **6**:3198–3207.
31 Haider MA, Van der Kwast TH, Tanguay J, Evans AJ, Hashmi AT, Lockwood G, *et al*. Combined T2-weighted and diffusion-weighted MRI for localization of prostate cancer. *AJR Am J Roentgenol* 2007; **189**:323–328.
32 Chenevert TL, Stegman LD, Taylor JM, Robertson PL, Greenberg HS, Rehemtulla A, *et al*. Diffusion magnetic resonance imaging: an early surrogate marker of therapeutic efficacy in brain tumors. *J Natl Cancer Inst* 2000; **92**:2029–2036.

33 Moffat BA, Chenevert TL, Meyer CR, Mckeever PE, Hall DE, Hoff BA, *et al*. The functional diffusion map: an imaging biomarker for the early prediction of cancer treatment outcome. *Neoplasia* 2006; **8**:259–267.

34 Woodhams R, Matsunaga K, Kan S, Hata H, Ozaki M, Iwabuchi K, *et al*. ADC mapping of benign and malignant breast tumors. *Magn Reson Med Sci* 2005; **4**:35–42.

35 Kartalis N, Lindholm TL, Aspelin P, Permert J, Albiin N. Diffusion-weighted magnetic resonance imaging of pancreas tumours. *Eur Radiol* 2009; **19**:1981–1990.

36 Kim H, Morgan DE, Buchsbaum DJ, Zeng H, Grizzle WE, Warram JM, *et al*. Early therapy evaluation of combined anti-death receptor 5 antibody and gemcitabine in orthotopic pancreatic tumor xenografts by diffusion-weighted magnetic resonance imaging. *Cancer Res* 2008; **68**:8369–8376.

37 Larsen SK, Solomon HF, Caldwell G, Abrams MJ. [99mTc]tricine: a useful precursor complex for the radiolabeling of hydrazinonicotinate protein conjugates. *Bioconjug Chem* 1995; **6**:635–638.

38 Lowry O, Rosebrough N, Farr L, Randall R. Protein measurement with the folin phenol reagent. *J Biol Chem* 1951; **193**:265–275.

39 Motulsky HJ, Christopoulos A. *Fitting models to biological data using linear and nonlinear regression*. San Diego: GraphPad Software Inc.; 2003.

40 Winzor DJ, Sawyer WH. *Quantitative characterization of ligand binding*. New York: Wiley-Liss; 1995.

41 Kim H, Morgan DE, Zeng H, Grizzle WE, Warram JM, Stockard CR, *et al*. Breast tumor xenografts: diffusion-weighted MR imaging to assess early therapy with novel apoptosis-inducing anti-DR5 antibody. *Radiology* 2008; **248**:844–851.

42 Kim H, Folks KD, Guo L, Stockard CR, Fineberg NS, Grizzle WE, *et al*. DCE-MRI detects early vascular response in breast tumor xenografts following anti-DR5 therapy. *Mol Imaging Biol* 2011; **13**:94–103.

43 Neter J, Kutner MH, Nachtsheim JC, Wasserman W. *Applied linear statistical models*. Columbus: The McGraw-Hill Companies, Inc.; 1996.

44 Hertzog C, Rovine M. Repeated-measures analysis of variance in developmental research: selected issues. *Child Dev* 1985; **56**:787–809.

45 Yang JM, O'Neill P, Jin W, Foty R, Medina DJ, Xu Z, *et al*. Extracellular matrix metalloproteinase inducer (CD147) confers resistance of breast cancer cells to anoikis through inhibition of bim. *J Biol Chem* 2006; **281**:9719–9727.

46 Bougatef F, Menashi S, Khayati F, Naimi B, Porcher R, Podgorniak MP, *et al*. EMMPRIN promotes melanoma cells malignant properties through a HIF-2alpha mediated up-regulation of VEGF-receptor-2. *PLoS One* 2010; **5**:e12265.

47 Kim H, Folks K, Guo L, Sellers JC, Fineberg NS, Stockard CR, *et al*. Early therapy evaluation of combined cetuximab and irinotecan in orthotopic pancreatic tumor xenografts by dynamic contrast-enhanced magnetic resonance imaging. *Mol Imaging* 2011; **10**:153–167.

48 Fiebig HH, Maier A, Burger AM. Clonogenic assay with established human tumour xenografts: correlation of *in vitro* to *in vivo* activity as a basis for anticancer drug discovery. *Eur J Cancer* 2004; **40**:802–820.

49 Escorcia FE, Henke E, McDevitt MR, Villa CH, Jones PS, Blasberg RG, *et al*. Selective killing of tumor neovasculature paradoxically improves chemotherapy delivery to tumors. *Cancer Res* 2010; **70**:9277–9286.

50 Bhattacharya A, Seshadri M, Oven SD, Toth K, Vaughan MM, Rustum YM. Tumor vascular maturation and improved drug delivery induced by methylselenocysteine leads to therapeutic synergy with anticancer drugs. *Clin Cancer Res* 2008; **14**:3926–3932.

51 Ichikawa K, Liu W, Zhao L, Wang Z, Liu D, Ohtsuka T, *et al*. Tumoricidal activity of a novel anti-human DR5 monoclonal antibody without hepatocyte cytotoxicity. *Nat Med* 2001; **7**:954–960.

52 Rajeshkumar NV, Rasheed Z, Garcia-Garcia E, López-Ríos F, Fujiwara K, Matsui WH, *et al*. A combination of DR5 agonistic monoclonal antibody with gemcitabine targets pancreatic cancer stem cells and results in long-term disease control in human pancreatic cancer model. *Mol Cancer Ther* 2010; **9**:2582–2592.

53 Fenster A, Downey DB. Cardinal HN three-dimensional ultrasound imaging. *Phys Med Biol* 2001; **46**:R67–R99.